Carbohydrate Polymers 318 (2023) 121132

Contents lists available at ScienceDirect

Carbohydrate Polymers

journal homepage: www.elsevier.com/locate/carbpol

Hornification of cellulose-rich materials – A kinetically trapped state

Farhiya Alex Sellman [a,c,*], Tobias Benselfelt [a,b,*], Per Tomas Larsson [a,c,d], Lars Wågberg [a,c,*]

[a] KTH Royal Institute of Technology, Department of Fiber and Polymer Technology, 11428 Stockholm, Sweden
[b] School of Materials Science and Engineering, Nanyang Technological University, 639798 Singapore, Singapore
[c] KTH Royal Institute of Technology, Department of Fiber and Polymer Technology, Wallenberg Wood Science Center (WWSC), 11428 Stockholm, Sweden
[d] RISE Research Institutes of Sweden, 11486 Stockholm, Sweden

ARTICLE INFO

Keywords:
Hornification
Cellulose nanofibril
Aggregation
Swelling
Kinetics

ABSTRACT

The fundamental understanding concerning cellulose-cellulose interactions under wet and dry conditions remains unclear. This is especially true regarding the drying-induced association of cellulose, commonly described as an irreversible phenomenon called hornification. A fundamental understanding of the mechanisms behind hornification would contribute to new drying techniques for cellulose-based materials in the pulp and paper industry while at the same time enhancing material properties and facilitating the recyclability of cellulose-rich materials. In the present work, the irreversible joining of cellulose-rich surfaces has been studied by subjecting cellulose nanofibril (CNF) films to different heat treatments to establish a link between reswelling properties, structural characteristics as well as chemical and mechanical analyses. A heating time/temperature dependence was observed for the reswelling of the CNF films, which is related to the extent of hornification and is different for different chemical compositions of the fibrils. Further, the results indicate that hornification is related to a diffusion process and that the reswellability increases very slowly over long time, indicating that equilibrium is not reached. Hence, hornification is suggested to be a kinetically limited phenomenon governed by non-covalent reversible interactions and a time/temperature dependence on their forming and breaking.

1. Introduction

The irreversible association of cellulose upon drying has been the subject of substantial research for many years. The consequences of this phenomenon are a shrinkage or collapse of the fiber wall, a lower water-holding capacity of fibres, reduced fiber flexibility, and increased brittleness of fiber-based materials. These irreversible structural changes are all characteristics of the process called hornification (Kato & Cameron, 1999), but despite considerable research efforts, the underlying mechanisms are still poorly understood.

Hornification is primarily induced by removing water from fiber walls (Laivins & Scallan, 1993), where elevated temperatures increase the water-removal rate. (Salmén & Stevanic, 2018) Based on this, different temperatures reflect different water evaporation and diffusion rates, degrees of molecular mobility in the cellulose networks, and final water contents after drying.

High-yield pulps, in which much of the lignin and hemicellulose matrix remains, are less susceptible to hornification. These polymers are suggested to act as spacers, preventing direct cellulose-cellulose contact and thus preventing association. (Hubbe, Venditti, & Rojas, 2007; Laivins & Scallan, 1993; Oksanen, Buchert, & Viikari, 1997) Removing most of the lignin and hemicellulose during delignification leads to a closure of the pores in the fiber wall already in the wet state. (Bristow & Kolseth, 1986).

The accessible surface area inside cellulose fibres is permanently reduced once hornification occurs. (Oksanen et al., 1997; Pönni, Rautkari, Hill, & Vuorinen, 2014) This loss of accessibility means that cellulose surfaces of fibres or fibrils and their chemical functionality are not efficiently utilized for further modification or integration with other material components. Therefore, in striving toward more eco-friendly structural materials from renewable resources, a fundamental understanding of the interactions behind hornification is essential for tailoring cellulose-based materials and composites. (Ansari, Sjöstedt, Larsson, Berglund, & Wågberg, 2015).

Understanding the mechanism(s) behind hornification is of great significance to processes where drying and rewetting of fibres are involved, as it affects the fiber quality. Indeed, the cellulose fiber-water relationship is fundamental to papermaking, and large amounts of money and resources could be saved if hornification was understood and prevented. (Benselfelt et al., 2023) The advantages of understanding the

* Corresponding authors at: KTH Royal Institute of Technology, Department of Fiber and Polymer Technology, 11428 Stockholm, Sweden.
E-mail addresses: fase@kth.se (F.A. Sellman), bense@kth.se (T. Benselfelt), wagberg@kth.se (L. Wågberg).

https://doi.org/10.1016/j.carbpol.2023.121132
Received 1 February 2023; Received in revised form 15 June 2023; Accepted 16 June 2023
Available online 19 June 2023

underlying mechanisms of hornification are numerous. It would contribute to new drying strategies for industries, more optimized utilization of fibres, improved product properties of cellulose-based materials, and could increase the recycling of fibres. (Čabalová, Kačík, Geffert, & Kačíková, 2011; Hubbe et al., 2007).

Several processes have been suggested to explain hornification, with the common enabling factors of water removal and elevated temperature. In Table 1, the most common hypotheses are summarized.

The proposed mechanisms of hornification include an increase in local ordering or co-crystallization of fibrils, (Kato & Cameron, 1999; Newman, 2004) the formation of crosslinking that is either covalent (Back & Klinga, 1963a; Back, Klinga, 1963b; Fernandes Diniz et al., 2004) or physical intermolecular hydrogen bonding that can withstand breaking upon rewetting. (Laivins & Scallan, 1993) However, the models that suggest the formation of hydrogen bonding between fibrils and an increase in crystallinity upon drying are not mutually exclusive, which is observed in the works of Peng et al. (Peng et al., 2013; Peng, Gardner, & Han, 2012) Beyond this, extensive structural characterizations have been performed on wood cell walls, pulp fibres and other cellulose-rich systems, such as cellulose hydrogel beads, to study drying-induced changes. (Karlsson et al., 2018; Li et al., 2020; Paajanen, Zitting, Rautkari, Ketoja, & Penttilä, 2022; Penttilä et al., 2021).

In the present contribution, carboxymethylated cellulose nanofibril (CNF) and hemicellulose-rich CNF (Holo-CNFs) films are used as model materials to study the irreversible association of cellulose-based materials upon drying at higher temperatures (105–150 °C) and for different times (0 - 4 h). By measurements of the degree of swelling, CP/MAS ^{13}C NMR, WAXS, XPS, multivariate FTIR and mechanical properties before and after the drying procedures, the changes exerted by these treatments on the CNF samples are evaluated in light of the suggested hornification mechanisms in the literature. Since hornification is postulated to be a surface phenomenon (Laivins & Scallan, 1993), the interactions associated with surfaces would consequently be more significant in materials comprising nanoscale building blocks. Despite significant modification of nanofibril surfaces, hornification is present, indicating that it is not specific to pure cellulose. Nanocelluloses can thus increase the response and hence the resolution of measurements compared to macroscopic fibres. With these model systems, it is also straightforward to investigate the influence of different surface modifications on hornification. As such, the counterions H^+, Li^+, Cs^+ and Mg^{2+} and their effect on the hornification of CNFs were explored as their different size and hydration may affect the contact between fibril surfaces, i.e. a larger or more hydrated ion may prevent close contact between fibrils and thus prevent or reduce hornification.

It should, however, be stressed that the CNFs are modified cellulose enriched with carboxylic acid groups, which means that only in certain aspects do they behave similar to unmodified cellulose. One difference and advantage is that sheets prepared from CNFs swell more than native cellulose, which means that the influence of hornification is easier to measure, and the resolution is increased. (Grignon & Scallan, 1980; Saito et al., 2009; Saito, Kimura, Nishiyama, & Isogai, 2007; Sjöstedt, Wohlert, Larsson, & Wågberg, 2015).

The collected results from the reswelling investigations in the current contribution show clear correlations between temperature, heating time, and extent of hornification for CNFs with different counterions. It has also been observed that films from fibrils with different chemical compositions, such as Holo-CNFs, show very different aging kinetics. Aging, in this sense, is used interchangeably with the heat treatment process. No chemical changes were detected as measured through XPS and multivariate FTIR analyses. Thus, it is argued that irreversible pore closure in cellulosic materials is due to physical interactions within molecular contact points.

What remains to achieve a complete understanding of hornification is an establishment of the true molecular mechanism behind the kinetically trapped cellulose/cellulose interactions, which requires critical experiments in which the diffusion of water molecules and possible entanglements of surface-bound polymer chains can be separated from interfacial adhesion interactions.

Table 1
Overview of hornification studies proposing different mechanisms.

Irreversible hydrogen bonding	Energy minimum by local ordering/co-crystallization	Formation of covalent bonds
"The mechanism of hornification of wood pulps" (Laivins & Scallan, 1993)	"Carbon-13 NMR evidence for cocrystallization of cellulose as a mechanism for hornification of bleached kraft pulp" (Newman, 2004)	"Reactions in Dimensional Stabilization of Paper and Fiber Building Board by Heat Treatment" (Back & Klinga, 1963b)
"A review of the relationship between thermally-accelerated aging of paper and hornification" (Kato & Cameron, 1999)	"CP/MAS ^{13}C NMR study of pulp hornification using nanocrystalline cellulose as a model system" (Idström, Brelid, Nydén, & Nordstierna, 2013)	"Hornification – its origin and interpretation in wood pulps" (Fernandes Diniz, Gil, & Castro, 2004)
"Highly transparent 100 % cellulose nanofibril films with extremely high oxygen barriers in high relative humidity" (Xia et al., 2018)		

2. Result and discussion

The uniaxial swelling of CNF films, fabricated through vacuum-filtration of aqueous dispersions, allows for easy measurements of the extent of hornification related to the ability of the CNF film to reswell after drying. (Benselfelt, Engström, & Wågberg, 2018; Benselfelt & Wagberg, 2019; Hatton, Engström, Forsling, Malmström, & Carlmark, 2017) As the smallest supramolecular structural unit of plant fiber, CNFs are an excellent model system for mimicking the structural changes in the macroscopic fiber wall upon water removal. (Wohlert et al., 2022).

Reswelling after heat treatment is a valuable guideline for when and to which extent hornification occurs. As a starting point, the irreversible association of cellulose-rich surfaces was studied by subjecting films of carboxymethylated CNFs and Holo-CNFs to heat treatments for different times and temperatures. The films were subsequently placed in water to equilibrate, and the thickness of the films in the reswollen state was measured to establish a connection between the reswelling ability, the internal CNF network structure through X-ray scattering and solid-state NMR measurements and possible molecular interactions from FTIR and XPS measurements resulting from the thermal treatment. In the present study, a relative reduction of the CNF films' degree of reswelling was interpreted as directly related to the degree of hornification. The swelling measurements used in this study quantify the water uptake in a similar way as the water uptake determined by fiber saturation point (FSP) measurements.

2.1. The effects of temperature and heating time on hornification

The swelling degree is defined as $\frac{d_{wet}-d_{dry}}{d_{dry}}$, where d_{wet} and d_{dry} represent the wet and dry thickness of the films. The ratio of the swelling degree without and after a thermal treatment, i.e. $\frac{Swelling\ degree\ after\ heat\ treatment}{Swelling\ degree\ before\ heat\ treatment}$, is herein termed reswelling after heat treatment. Both are relative measurements used to describe the effect of temperature and heating time on the swelling of the CNF films and hornification.

The reswelling after heat treatment as a function of heating time and temperature in Fig. 1 shows that elevated temperature and prolonged heat exposure reduce the reswelling, i.e., a higher degree of hornification. This behaviour is not apparent for CNF-H^+ films, which will be

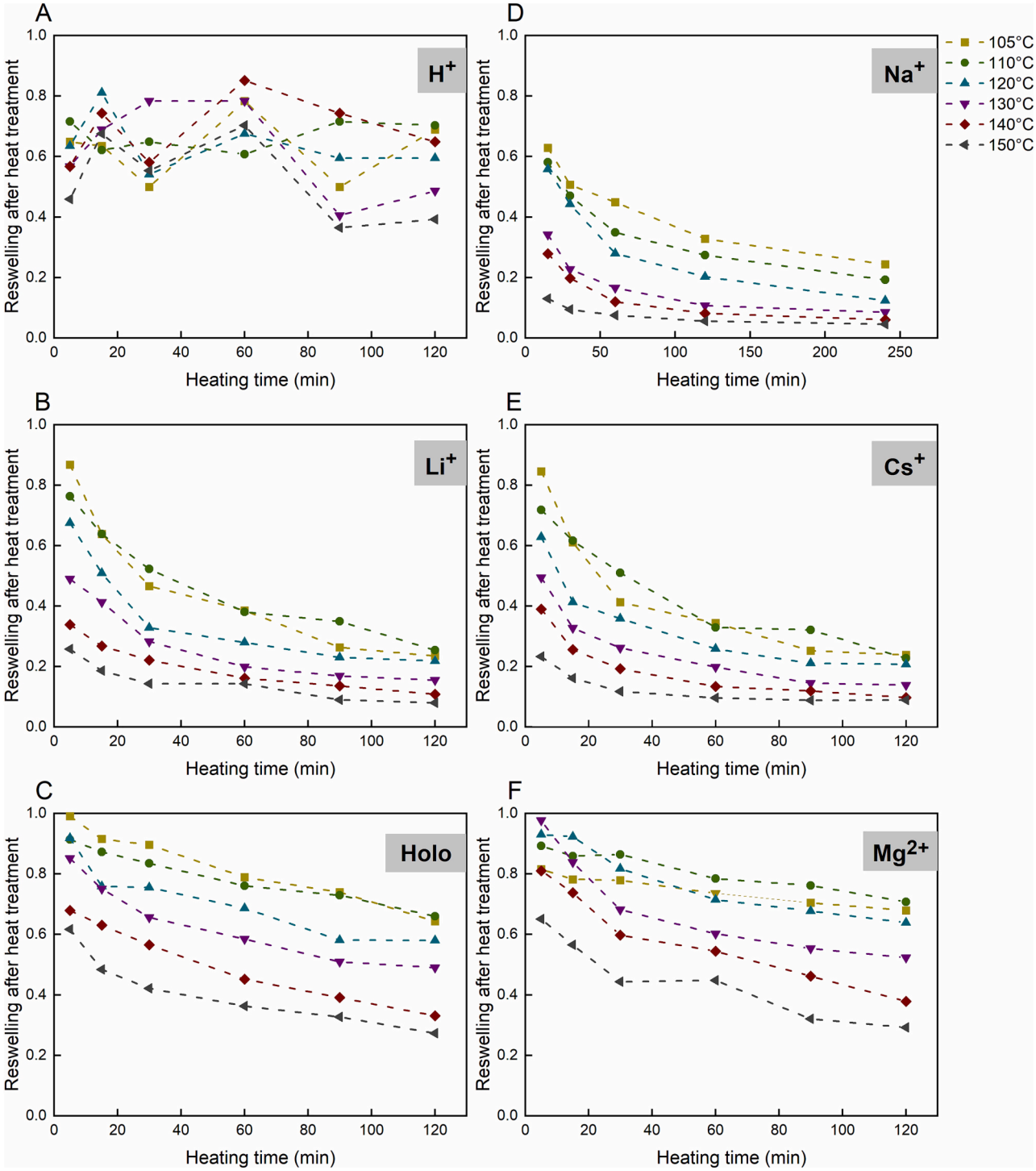

Fig. 1. Aging-reswelling curves for CNF films of different compositions. The reswelling after heat treatment is relative to the swelling degree of the respective reference CNF film (Fig. 2). The lines in the figure should merely be regarded as a guide to the eye.

dealt with later. The shape of the reswelling curves in Fig. 1 indicates that the aging-reswelling kinetics follow different orders depending on the chemical composition of the CNF films. However, except for CNF-H^+, they all exhibit significant time-dependent aging in the temperature intervals of 105–150 °C.

The difference between the CNF samples lies in their surface charge density and composition, which affects their initial swelling before heat treatment. CNF-Na^+ (or Li^+, Cs^+, Mg^{2+}) and CNF-H^+ are carboxymethylated CNFs, the former having dissociated carboxyl groups and the latter in acid form. When the carboxylate groups are protonated, the charged fibrils are neutralized, which changes the chemical environment of the fibril surface. In contrast, Holo-CNFs are cellulose fibrils covered by hemicelluloses (Yang, Berthold, & Berglund, 2018), i.e., short-chained and disordered polysaccharides. A comparison of the swelling thickness of reference CNF films in Fig. 2, shows that the order of swelling follows previous studies (Benselfelt, Nordenström, Hamedi, & Wågberg, 2019) according to:

$$Li^+ > Na^+ > Cs^+ > Mg^{2+} \geq \text{Holo} >> H^+$$

Several contributing factors control the water uptake in cellulose gel

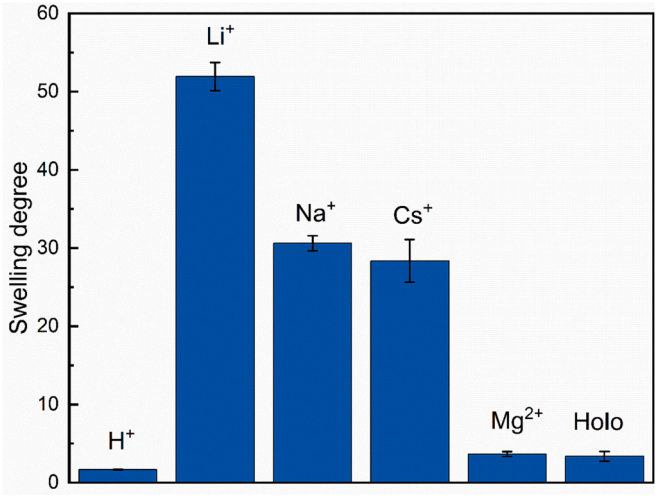

Fig. 2. The swelling degree of reference CNF films with different counterions and Holo-CNF after 24 h equilibration in water relative to the thickness of the corresponding dry film. The error bars are standard deviations.

networks, in a similar way as described by Flory for polyelectrolyte gels (Flory, 1953) based on the Flory-Huggins theory for polymer solutions (Flory, 1942; Huggins, 1941) with additional terms representing the ionic contributions and the restraining network contributions. The swelling owing to ionic contributions in cellulose-based networks has been previously quantified in the literature. (Tobias Benselfelt, Nordenström, Hamedi, et al., 2019; Karlsson, Larsson, Hansson, & Wågberg, 2019; Lindström & Carlsson, 1982) Charged groups, in this case, dissociated carboxylic acid, lead to an osmotic pressure that expands the network. (Grignon & Scallan, 1980) When the ionic contribution is eliminated by decreasing pH of carboxylic acid containing networks, as for CNF-H^+ films, some water uptake still remains, which is assigned to the non-ionic contributions to the swelling related to the ability of the macromolecular network to mix with water, i.e., the thermodynamics of mixing. (Flory, 1942; Grignon & Scallan, 1980; Huggins, 1941).

A low swelling degree is expected in H^+ form (Fig. 1A) due to the dramatically reduced osmotic pressure inside the network. As a result, significant errors are found in the relative reswelling degree since the difference between reference and heat treated samples is small. For the other monovalent counterions Na^+, Li^+ and Cs^+ (Fig. 1B, D-E), the same temperature/time dependence on the reswelling degree is observed. One implication of this is that the specific ion (Na^+, Li^+ or Cs^+) effects/hydration energies of these cations do not have a significant impact on the aging process, and the focus will be narrowed down to Na^+ in following discussion.

A less pronounced and linear temperature/time dependence is noted with Holo-CNF, and reasonably so since hemicellulose coverage is expected to reduce the effect of thermal treatment, i.e., the extent of hornification. (Oksanen et al., 1997) Nevertheless, a reduced water uptake can be explained by an incomplete hemicellulose coverage, which would still allow for cellulose surfaces to coalesce where the cellulose surfaces are exposed. Other studies found that the extent of hornification of kraft pulp fibres is progressively reduced by increasing amounts of adsorbed glucuronoxylan, (Köhnke, Lund, Brelid, & Westman, 2010) which also highlights the importance of an adequate coverage of fibril surfaces for efficient prevention of cellulose association.

The introduction of a divalent counterion (Fig. 1F) induces interfibrillar attractions in the CNF network. (Benselfelt, Nordenström, Hamedi and Wågberg, 2019; Benselfelt, Nordenström, Lindström, & Wågberg, 2019) Although a temperature/time dependence on the reswelling degree is found, multivalent ions noticeably prevent the network from collapsing upon aging and thus limits the degree of hornification.

The same aging-reswelling behaviour displayed for CNF-Na^+ was observed for cellulose hydrogel beads consisting of regenerated cellulose in water, see Fig.S1. In contrast to the CNF networks, cellulose hydrogel beads are non-crystalline, molecularly dispersed cellulose polymers (Karlsson et al., 2018), indicating that the ordering of cellulose in semi-crystalline fibrils is not a requirement for hornification.

The influence of heating time on the degree of reswelling is of particular interest, as increasing treatment time results in lower reswelling. A simple exponential relationship is introduced to describe the film swelling after aging, using the generalized empirical expression defined by Ritger and Peppas (Ritger & Peppas, 1987), which has previously been adapted for the swelling of cellulose nanocrystal thin films (Reid, Kedzior, Villalobos, & Cranston, 2017):

$$\frac{M_t}{M_\infty} = \frac{d_{wet} - d_{dry}}{d_{dry}} = Swelling\ degree = kt^n \quad (1)$$

Where k is a constant characterizing the polymeric network, M_t and M_∞ are the volume of water within the swollen network after time t and after an infinite amount of time. Fickian diffusion is defined by $n = 0.5$. However, since the present work is focused on investigating the influence of heating time on the degree of reswelling, an inverse relation is obtained between the degree of swelling and the heating time that induces hornification ($reswelling\ degree \propto \frac{1}{Heating\ time}$). n-values of −0.5 could hence be indicative of a hornification process that is based on molecular diffusion.

As shown in Fig. 3 there is an almost linear relationship between the reswelling after heat treatment and $t^{-0.5}$, which indeed indicates that hornification is diffusion-controlled for CNF-Na^+ films. In this respect, the two molecular species that might diffuse during heating are water or the glucan/modified glucan polymers on the CNF surfaces. The oxidized glucan chains on the fibril surfaces will have higher mobility in the wet state. (Garg, Linares, & Zozoulenko, 2020) However, before the aging processes/experiments are started all the films have been mildly dried during film formation, which means that the surface polymers will be severely confined and would hence show a limited Fickian diffusion behaviour, (Crank, 1979) indicating that the remaining water in the films is the vital diffusing elements that will show increased molecular mobility at elevated temperatures. Furthermore, the Holo-CNFs, which are covered with hemicellulose from the wood, could show a different behaviour since the lower molecular mass and non-ordered hemicellulose should be more mobile even at low moisture contents and as can be seen in Fig. 2 the change in degree of swelling for these materials is much lower as compared to the more highly swollen systems.

When the aged films are allowed to reswell over much longer times (≥1 year), a continous increase in the swollen thickness can be measured, which is presented in Fig. 4. However, this increase occurs on a much slower timescale compared to the initital immersion of an aged film, where the major swelling takes place within minutes to hours. Fig. S2 shows that the swelling degree of a CNF-Na^+ film does not saturate after a week and increases over at least four weeks, this continues up to a year but very slowly. The swelling of the reference samples (at heating time = 0 min) increases the most over time. The long-term increase in swelling is generally highest for Holo-CNF, seen in Fig. 4B, which is reasonable due to the more favorable hydration of hemicelluloses. (Takamura, 1968) Moreover, these polymers can not pack as tightly because of their branched and disordered nature, which may allow water molecules to penetrate the structure more easily over time. (Sun, Sun, & Tomkinson, 2004).

The above data suggest that the displacement of water from the network by diffusion during heating might be the primary cause of hornification, allowing the cellulose surfaces to come in close molecular contact. It does not, however, clarify which interaction mechanisms between the cellulose surfaces are responsible for the strong, pseudo-

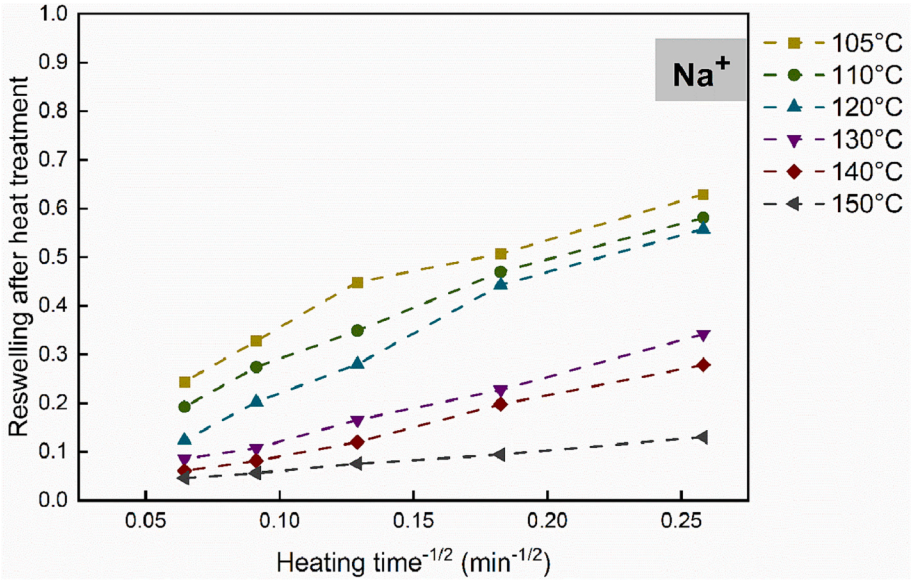

Fig. 3. Reswelling after heat treatment as a function of $t^{-0.5}$ of aged CNF-Na^+ films.

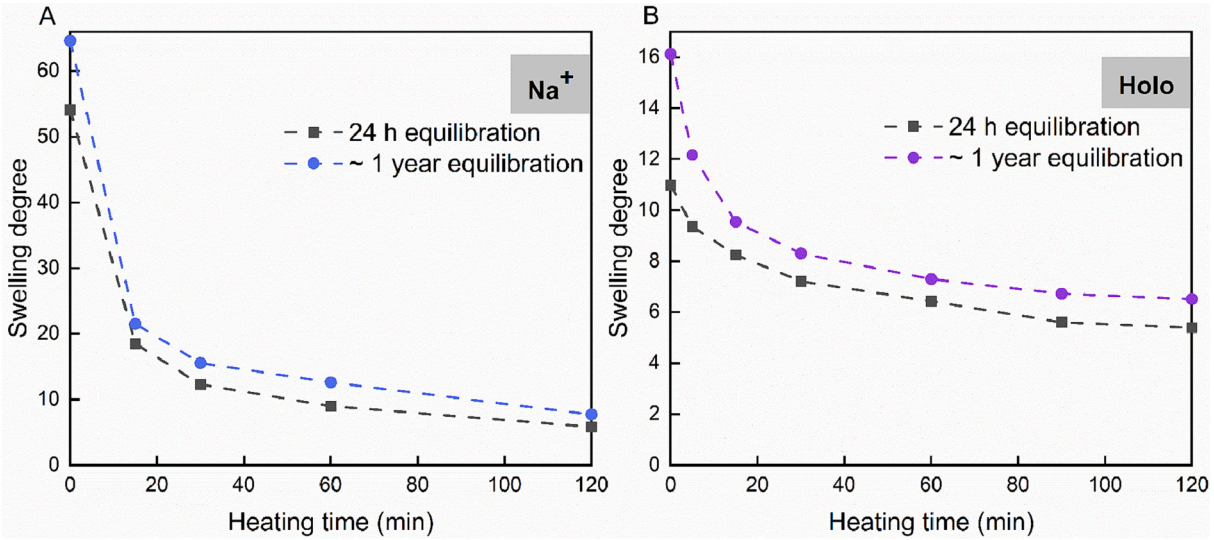

Fig. 4. Comparison of the swelling degree after 24 h and ~1 year for A) CNF-Na^+ and B) Holo-CNF aged at 130 °C.

irreversible interaction after the removal of all the water molecules. These data also suggest that diffusion of water back into the network is a prolonged, kinetically hindered process, meaning there would be a large hysteresis between the deswelling and reswelling processes. This description indicates that hornification might be fully reversible over infinite time and one objective of future studies could aim to shorten this reswelling time in scalable processes. Note that CNFs form entangled networks that must be disentangled for complete redispersion, and this would require some agitation.

The following sections are dedicated to a detailed structural and chemical analysis of reference and heat treated samples to find the molecular interaction responsible for the above-mentioned behaviour.

2.2. Structural characterization of aged CNF films

One of the suggested molecular mechanisms behind the hornification, mentioned in Table 1, is a *co*-crystallization of glucan polymers in which the coalescence of neighbouring cellulose fibril surfaces results in an increase in the degree of crystallinity. (Idström et al., 2013; Newman, 2004) This mechanism implies that the relation between the number of non-ordered surface polymers and the number of highly ordered polymers of the fibril core, should be affected due to hornification. In order to determine the supramolecular structure of the different samples at different degrees of hornification, CP/MAS ^{13}C NMR was applied. Fig. 5 presents the full spectra for differently treated samples with regions corresponding to the different carbons in the glucose unit marked above. The C-4 and C-6 signals are assigned to the surfaces and interiors of crystalline domains, respectively, and are labelled as *s* and *i*.

Signal intensity changes occurring due to the drying procedures are expected in surface regions as the crystalline interior of the cellulose fibril is unchanged by elevated temperatures in the chosen interval. The CP/MAS ^{13}C NMR spectra of a reference CNF-Na^+ film and films dried at 130 °C and 150 °C in Fig. 6A-B show no spectral changes of the C-4 signals at elevated drying temperatures. The lack of spectral change means that no detectable change in the degree of cellulose ordering (crystallinity) is accompanying the heat treatment.

The reference CNF-Na^+ film had a lower signal-to-noise ratio possibly due to a higher water content, with more stray fields induced by

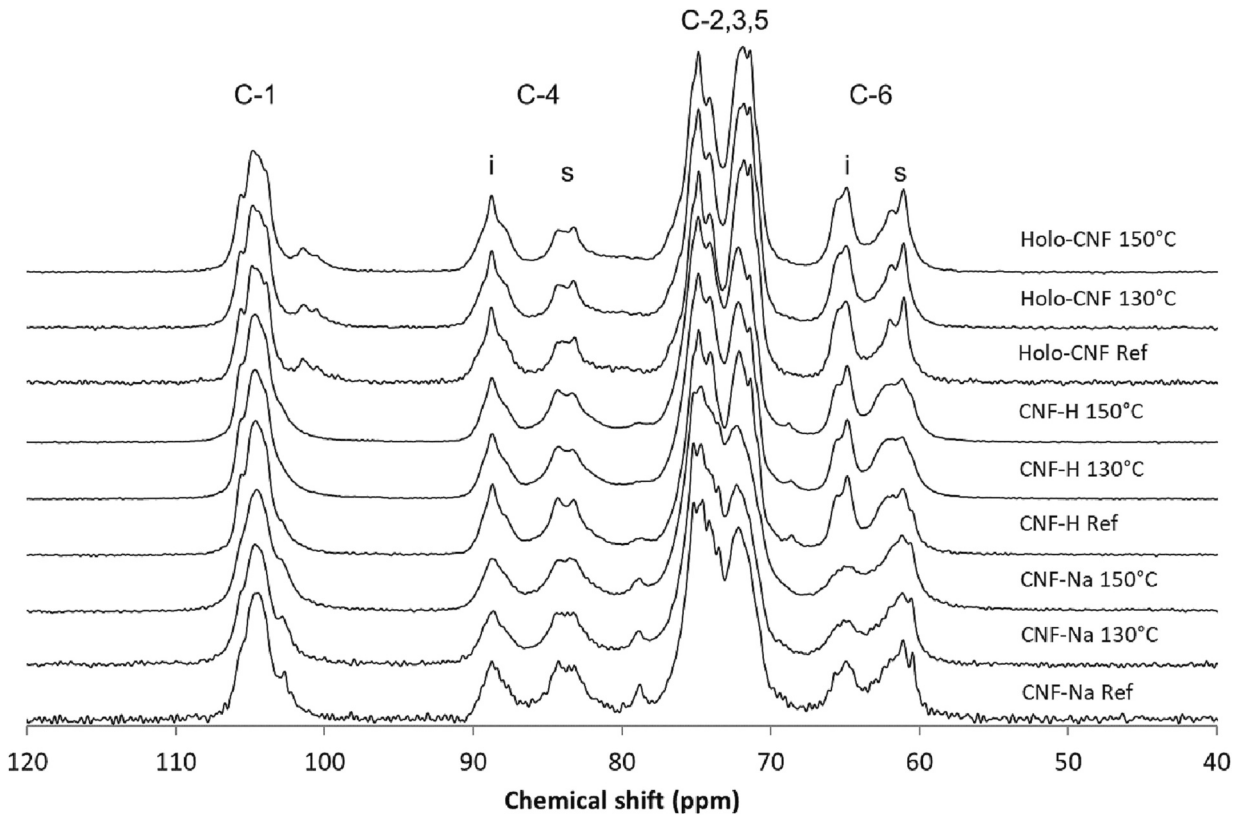

Fig. 5. CP/MAS ^{13}C NMR spectra of water-swollen CNF films. The films were first heat treated for 4 h at the temperatures shown above each spectrum and subsequently reswollen. The reference samples did not undergo any additional drying beyond film formation which is a mild drying at 93 °C for 20 min.

the presence of mobile Na^+ ions. This can decrease the efficiency of the cross-polarization with a consequent loss in signal-to-noise, especially noticeable in the C-6 region, around 65 ppm. The signal around 102 ppm, most evident in the Holo-CNF samples, was assigned to hemicellulose, most probably glucomannan. (Newman, 2004) Fig. 6 shows the overall structural characterization for CNF-Na^+ films in the reference and the aged states. The signal position in solid-state NMR depends on polymer conformation and the typical cellulose I spectrum consists of six signals from AGU, split into clusters owing to the supramolecular structure of the cellulose I fibril. (VanderHart & Atalla, 1984) The positions of the signals remain relatively fixed regardless if CNFs or pulp fibres are used in the measurement. (Larsson, Wickholm, & Iversen, 1997) However, when using WAXS to evaluate the crystalline ordering of the glucan chains in the fibres or fibrils it must be kept in mind that the X-ray scattering is sensitive to plane distances in the crystal lattice. Plane distances may change without significantly altering polymer conformation. A comparison between the sharp, distinct signals of cotton linters owing to the reflections (110), (1−10), (102) and (200) to that of CNFs in Fig. 6C indicates that the CNF films have a broadened and, in some cases, shifted positions compared with signals from a typical cellulose I lattice. The signal broadening indicates a broader distribution of plane distances in the CNF networks, indicating less ordered fibrillar interiors. (Scherrer, 1918).

The results from the CP/MAS ^{13}C NMR measurements also show that the drying at 150 °C lead to a significant increase in the lateral fibril aggregate dimension (LFAD) as shown in Fig. 6D for CNF-Na^+ and this is also the case for CNF-H^+ and Holo-CNF (Table S1). It has previously been shown that fibril aggregate dimensions increase due to drying of pulp fibres. (Hult, Larsson, & Iversen, 2001; Salmén & Stevanic, 2018) However, no such effect was observed when drying at 130 °C. Holocellulosic nanofibrils have a larger lateral fibril dimension (LFD) than the carboxymethylated CNFs, which is reasonable due to the chemical modification of the CNFs and the arrangement of hemicellulose in Holo-CNF as a cellulose-hemicellulose core-shell structure. (Yang, Reid, Olsén, & Berglund, 2019) As determined by solid-state NMR, the crystallinity was not affected by drying at elevated temperatures. From WAXS measurements, only CNF films in their proton form showed a slight signal narrowing upon drying at 150 °C (Fig.S4), indicating a minor increase in the degree of order in the fibril interior.

2.3. Chemical analysis

In order to evaluate the possible formation of interfibrillar covalent bonds after heat treatment, one of the hypotheses stated in Table 1, chemical analyses were performed using X-ray photoelectron spectroscopy (XPS) and Fourier transform infrared (FTIR) spectroscopy combined with multivariate analysis. Traditionally, the difficulty of assessing an evolution of suggested covalent bonds upon hornification, such as esterification, has been due to the overlap of carboxyl carbonyl and ester carbonyl regions, occurring in both wavenumber (FTIR) (Pantze, 2006) and binding energies (XPS). Adding to the complexity is that the potentially formed ester bonds, which are catalysed in acidic conditions, would also be reversible by hydrolysis. (Pantze, 2006).

There was no principal difference in the C 1 s XPS spectra after drying for different durations (30, 60 and 120 min). The results in Table 2, showing the atomic ratios before and after heat treatment in the severest condition (150 °C, 2 h), suggest a small increase in O-C-O and C-OH bond. It should also be mentioned that aging the CNF films under such harsh conditions caused yellowing of the films, which did not occur at lower temperatures, and may indicate the formation of covalent bonds. (Ahn et al., 2019) Aging as a function of heating time did not produce any strong trends in terms of the increase in O-C-O and C-OH bonds (Table S2) for CNF-Na^+ and the small variations are, therefore, difficult to interpret.

The multivariate analysis procedure, following a procedure given elsewhere (Nylander, Svensson, Josefson, Larsson, & Westman, 2019),

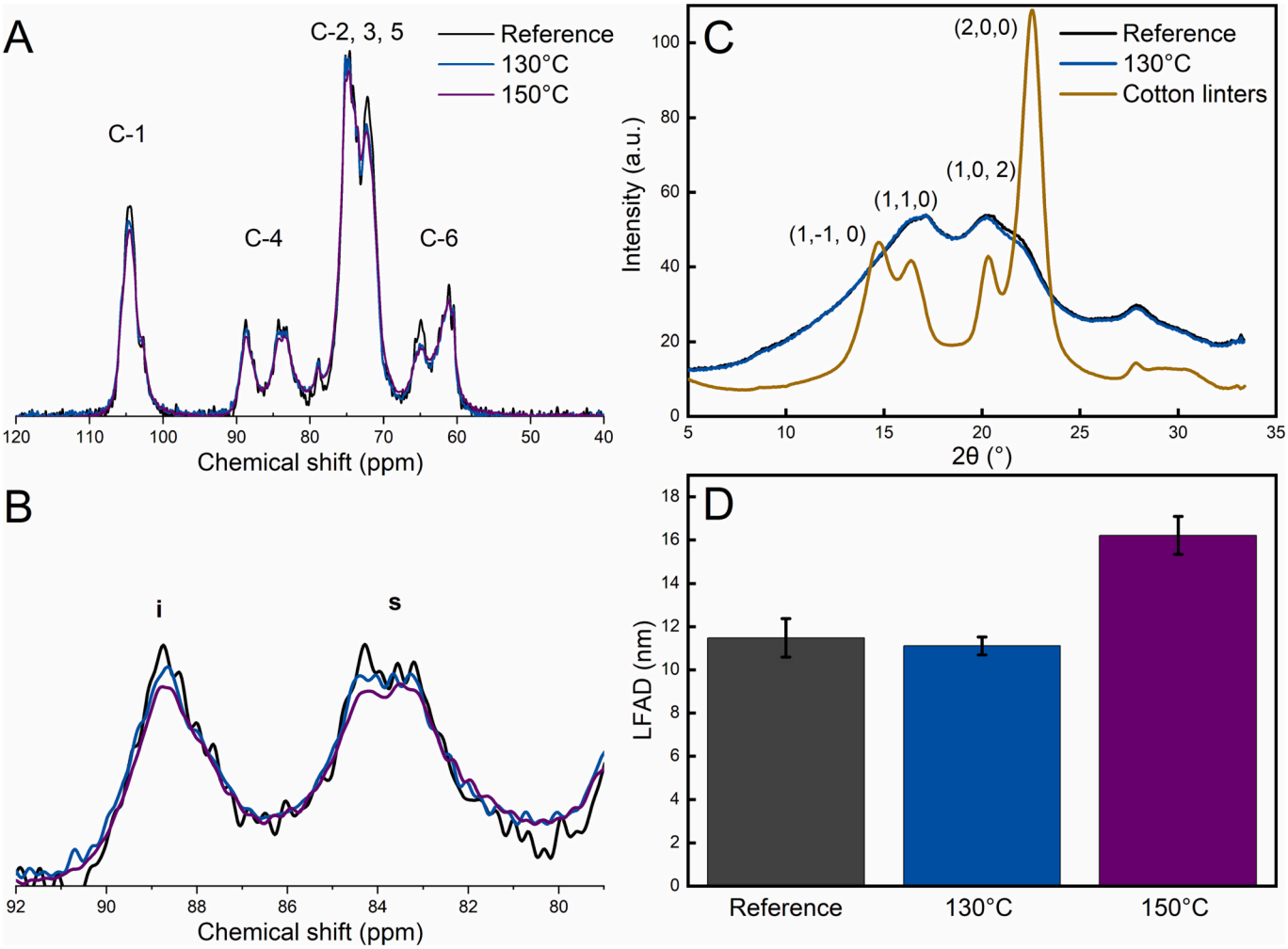

Fig. 6. Structural characterization of reference and aged for 4 h CNF-Na$^+$ films in comparison to a cotton sample showing: A) CP-MAS ^{13}C NMR spectra for the reference and aged CNF-Na$^+$ in the water-swollen state. B) Enlargement of the C4 region in A. C) WAXS intensities for the reference and aged CNF-Na$^+$ in the dry state compared to a cotton linter sample with high cellulose content. D) Changes in lateral fibril aggregate dimension (LFAD) for the reference and aged CNF-Na$^+$ depending on the heating temperature.

Table 2
Atomic ratios of the carbon chemical states in the different CNF films (before and after heat treatment) determined from C 1 s XPS presented in Fig.S5. Relative errors in these ratios are about 8–10 %.

Sample	Atomic ratios		
	C-OH	O-C-O	O=C-OH
CNF-Na$^+$ reference	15.9	3.1	1
CNF-Na$^+$ 150 °C 2 h	15.7	3.7	1
CNF-H$^+$ reference	14.2	2.9	1
CNF-H$^+$ 150 °C 2 h	17.7	4.2	1

consisted of a principal component analysis (PCA) and orthogonal projection to latent structures (OPLS) applied for the FTIR spectral data of CNF-Na$^+$, CNF-H$^+$ and Holo-CNF films that were heat treated for the different times and temperatures corresponding to Fig. 1. A PCA score plot of all heat treated samples and references is presented in Fig.S8. PCA is an unsupervised method, and the components PC1 and PC2 demonstrate the largest variation between spectra. The PCA score plot tells whether individual spectra are similar to each other or not, and the distance between spectra in the score space is related to their degree of similarity.

The OPLS spectral loadings in Fig.S9 and Fig.S10 reveal differences in spectra related to the heating temperatures, presenting the changes in spectral patterns for 105–140 °C and 150 °C, respectively. Separate OPLS were made for the respective chemical compositions at 105–140 °C and 150 °C since, at the highest temperature, samples showed unique spectral variations that did not follow the trend for lower heating temperatures. It is also seen from Fig.S8 that samples treated at 150 °C differed the most from the reference samples.

For 105–140 °C, the results from these measurements mainly reveal a decreased intensity in OH-vibrations in the 3000–3600 cm^{-1} region (Liang & Marchessault, 1959) as the aging intensifies, i.e. prolonged heating times or higher temperatures, suggesting changes related to the hydration water in the aged films. A slighter decrease at 2890 cm^{-1} attributed to C—H vibrations (Liang & Marchessault, 1959) was also observed. For CNF-H$^+$, these changes were accompanied by a decrease in the absorption band at 1737 cm^{-1}, related to the carboxylic acid group. For all CNF compositions heat treated at 150 °C, an increased intensity at 1737 cm^{-1} is observed. Additionally, CNF-Na$^+$ shows the same spectral changes from the heat treatment at 105–140 °C. However, for CNF-H$^+$ and Holo-CNF, an increase in the absorption bands at 3000–3600 cm^{-1} and 2890 cm^{-1} is instead observed at 150 °C. These results are summarized in Table S6.

Combined, these observations indicate that aging occurs without substantial chemical reactions up to 140 °C. Above this temperature, and in agreement with XPS measurements, it seems reasonable that some chemical reactions occurs that also provide a noticeable yellowing.

If these are crosslinking reactions contributing to hornification is difficult to tell, but the increased intensity of 1737 cm^{-1} could indicate ester or hemiacetal crosslinks. The reactions that take place at higher temperatures (150 °C) could also be related to thermal degradation of the nanocellulosic samples. Although the thermal decomposition of cellulose is known to occur above 200 °C, the thermal stability of nanocellulose has been shown to decrease as a consequence of chemical treatments and specifically the introduction of carboxylic acid groups, processing conditions such as homogenization and drying procedures. (Lichtenstein & Lavoine, 2017; Peng et al., 2013; Quiévy et al., 2010) Additionally, it has been demonstrated that the decomposition temperature for Holo-CNF films is above 200 °C. (Yang et al., 2019) These changes are, however, not a central part of hornification, as hornification is observed at lower heating temperatures.

2.4. Dry and wet tensile modulus of aged CNF films

The considerable change in the degree of swelling of the CNF sheets as a function of aging time and temperature indicates changes in the macroscopic properties of the CNF films. In order to evaluate if the aging impacts the mechanical properties of the sheets, their dry and re-wet tensile properties were evaluated. Differences in the mechanical properties of the sheets could also give indications/explanations about the molecular mechanism behind the detected aging.

The dry tensile properties as a function of heating time and temperature show no apparent trends (Fig.S6). The differences are within the accuracy limits for the different CNF films. However, it should be noted that the strain-at-break was higher for several heat treated films than the corresponding reference values. A higher strainability may not be expected if hornification results from an increased ordering/co-crystallization of the nanofibrils, which would be detected as an increased stiffness/brittleness. The dry tensile strength of Holo-CNF films is significantly higher than for the other CNF forms, which is related to their higher aspect ratio due to a well-preserved fibril structure and facilitated fibril-fibril joint strength induced by hemicelluloses surrounding the cellulose fibrils. (Benselfelt et al., 2018; Yang et al., 2019) Thus, the structural changes that occur once CNFs are dried at an elevated temperature do not seem to be reflected in the dry tensile properties of the films, irrespective of the chemical composition of the sample groups: ionized, protonated or hemicellulose-rich. Hence, the dry tensile properties of the films seem to be dominated by the network properties more than by specific interfibril interactions.

The stress-strain properties of the heat treated CNF films in a wet state are shown in Fig. 7A and summarized in detail in Table S3, and presented for the dry state in Table S4. Reference states for the rewetted films were not possible to evaluate due to a too high reswelling thickness of CNF-Na^+ and Holo-CNF, making them too weak to clamp for tensile testing.

Upon rewetting the aged films, there is a clear trend in the increase of wet strength and stiffness as a function of heating time, regardless of the CNF form. An increase in wet strength could indicate a resistance to water penetration, i.e., more water-resilient joints between the fibrils are formed, which is most apparent in the rewetted state for the aged CNF-H^+ films. These show a remarkably high average wet strength of 44.9 MPa upon heating for 2 h at 130 °C. Other studies have shown relationships between wet mechanical properties and specific ion effects in CNF networks (Tobias Benselfelt, Nordenström, Lindström, et al., 2019), as well as the influence of local acidic environments, which leads

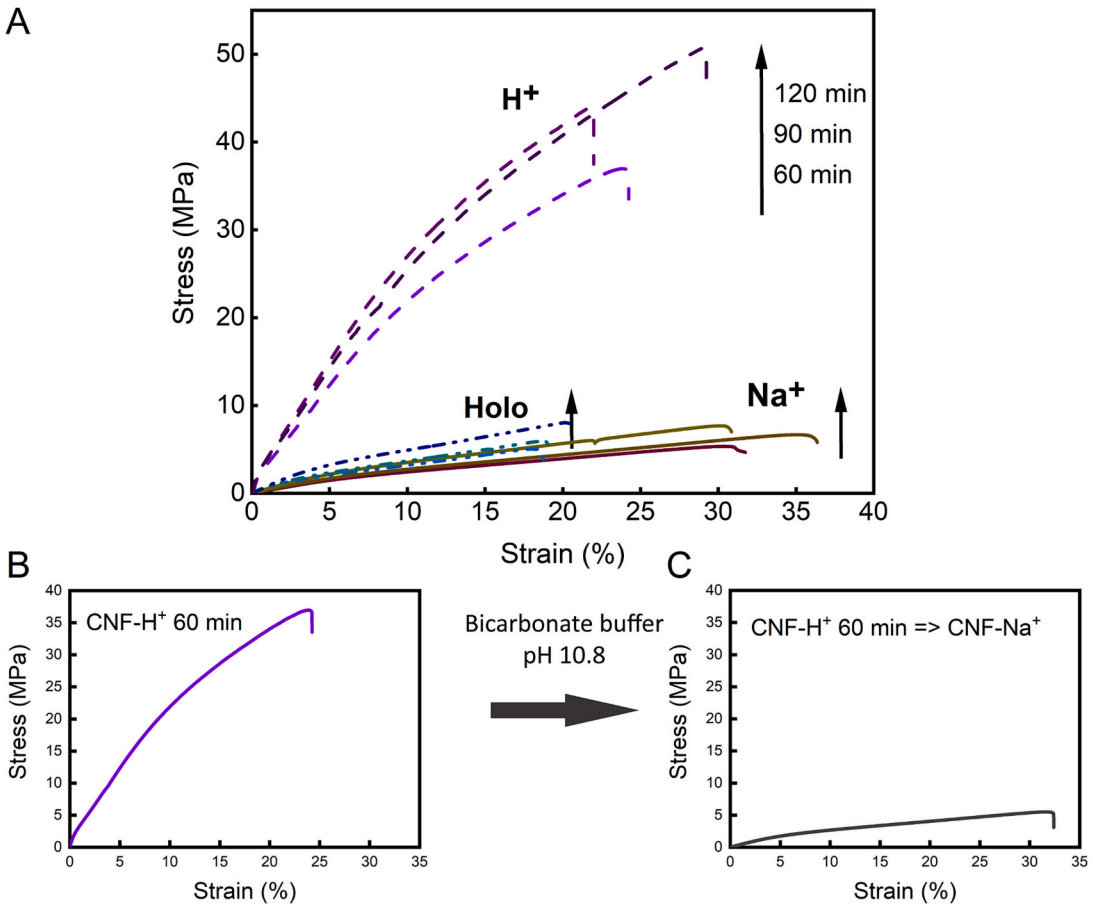

Fig. 7. Representative engineering stress-strain curves for the different films in the wet state for A) films aged for 60, 90 and 120 min at 130 °C. B) A film aged with the charges in their proton form (60 min, 130 °C) and C) ion-exchanged back to their sodium form.

to lower water uptake and improved mechanical integrity in water. In a previous work (Tobias Benselfelt, Nordenström, Lindström, et al., 2019) it was possible to establish a direct relationship between the change in wet moduli of these networks and a change in the solidity (ϕ) of the networks according to $E \propto \phi^4$. The solidity is proportional to the reciprocal of the swelling and is measured as the ratio between the dry and wet thickness of the CNF films. This finding indicates that the network density dictates wet mechanical properties rather than the specific chemistry behind the water uptake.

To assess whether the difference in mechanical properties between CNF-Na^+ and CNF-H^+ is a combined effect of the absence of charged groups and drying with heat or only due to the latter, an ion-exchange procedure was performed for films aged in protonated form. CNF films were formed in Na^+ and H^+ form and heat treated for 60 min at a temperature of 130 °C. The CNF-Na^+ films were then subsequently immersed in water for 72 h for swelling prior to the tensile measurements. The protonated films however, were placed in a carbonate-bicarbonate buffer (pH 10.8) for counterion exchange to Na^+. After washing, the CNF-H^+ film subjected to ion exchange (CNF-H^+ ≥ CNF-Na^+) were swelled in water before tensile testing. Fig. 7B shows the wet CNF-Na^+ films formed in Na^+-form and H^+-form, respectively, displaying similar tensile properties and reswelling degrees in Na^+-form. This data indicates that the regions of the fibril surfaces affected by the deprotonation are still accessible to ion exchange, despite the heat treatment, once the charged groups are converted back to their Na^+ form. Upon hornification, molecular contact points are established between fibrils, which occurs both for the CNF-H^+ and the CNF-Na^+ films. Following the ion exchange of the heat treated films from H^+ to Na^+, the formed joints give the same final properties regardless of counterion form during aging, which means that hornification occurs similarly for CNF-Na^+ and CNF-H^+ films. Thus, the apparent difference in the reswelling curves detected for CNF-H^+ and CNF-Na^+ respectively (Fig. 2A, D) seems to be solely due to the removal of surface charges and, consequently, due to differences in the osmotic swelling pressure for the different ionic forms, similar to what was shown by different multivalent counter ions. (Tobias Benselfelt, Nordenström, Lindström, et al., 2019).

2.5. Discussion about the hornification mechanisms

The different results from the aging studies have indeed demonstrated the complexity of the hornification process of cellulose-rich materials but also shown new insights and similar trends by using the nanofibril sheets with their high specific surface area. First, the investigation of the reswelling degree of the films after different aging temperatures and times indicates that the hornification is linked to a diffusion process. Since the aging is performed after a drying during the preparation of the sheets, it is still reasonable to assume that the primary diffusing component in these materials is water. This removal of the water no doubt brings cellulose surfaces into intimate proximity and molecular contact, and secondary diffusion processes of, for example, less ordered glucan chains in these contact zones cannot be ruled out, as this has been shown for other surface-bound polymers. (Maeda, Chen, Tirrell, & Israelachvili, 2002) The wet and dry mechanical testing of the differently aged CNF sheets has also shown similar and complementary trends. The aged films all show a significant wet strength and the samples aged with the carboxyl groups in the protonated form have a high wet tensile strength and wet modulus. However, after ion-exchange of the carboxyl groups back to the Na^+-form, these sheets show the same wet strength as those aged with the carboxyl groups in their Na^+-form, indicating that the remaining hornification occurs in the regions where the cellulose surfaces have been brought into close contact and that this process has not occurred in the areas containing the bulkier COO^- or COOH groups. This mechanism is depicted in Fig. 8 and indicates that adding carboxylate groups to cellulose surfaces has effectively reduced hornification.

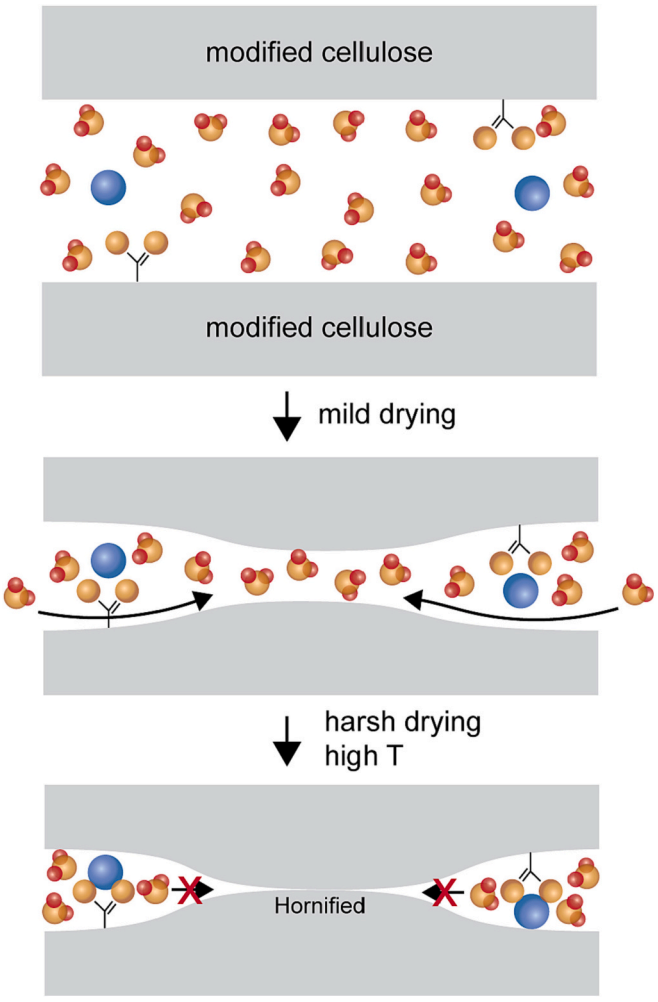

Fig. 8. Illustration of the preserved availability of carboxylate/carboxylic acid group upon drying. Blue spheres can be a counterion or a closely associated H^+ that would mainly dictate swelling pressure but have a little influence on interfibril interactions.

The different pattern in hornification of the holocellulose films also stresses the importance of an intimate cellulose/cellulose contact for developing a higher degree of hornification. The fact that there is a hornification for the networks from holocellulose fibrils indicate that the surface coverage of the hemicellulose is not complete but this suggestion indeed needs further investigations. Alternatively, it may also indicate that hornification is a general phenomenon, but the disordered hemicellulose hornify to a lower degree due to their elevated accessibility to water. The extent of hornification can also be mitigated by additives such as glycerol (Moser, Henriksson, & Lindström, 2018), carboxymethylated cellulose (Benselfelt et al., 2023; Butchosa & Zhou, 2014) or even in the presence of NaCl (Missoum, Bras, & Belgacem, 2012), which are proposed to act as blockers/spacers between fibrils, to prevent close contact and allow water to reenter.

The exact molecular mechanism responsible for the aging, did not involve substantial chemical reactions and permits a slow increase in reswelling during prolonged storage of the aged CNF films in water. This gradual diffusion of water back in to the aged CNF films reveals that the fibrillar networks have not reached an equilibrium state and that there is a kinetic barrier that needs to be overcome. Thus, hornification is suggested to be a kinetically trapped state, even though not necessarily entirely reversible.

The possible interactions behind this state and that hold the fibrils together are presented: electrostatic (hydrogen bonding and other polar

bonds), electrodynamic (van der Waal) interactions, or solvophobic effects. Hornification has previously been explained as irreversible hydrogen bonding between fibrils, but hydrogen bonds already exist in a water-soluble state against water with no significant enthalpy difference between the associated and the dispersed state of the fibrils. (Wohlert et al., 2021) If the fibril surfaces are close enough, i.e. at a molecular distance, van der Waal forces, which are always present, will have a dominating contribution to the interaction energy compared to hydrogen bonding. For complete contact, the water layer has to be removed, which is gradually achieved by heating. In colloidal science there is a frequently observed behaviour called hydration forces – a mechanism in which a thin water layer prevents two surfaces from reaching van der Waals contact even when forced together. (Israelachvili & Wennerström, 1996) Disrupting or removing the hydration layer is needed for strong van der Waals contacts, which could be what is happening during aging. Highly hydrated charged groups found on carboxymethylated CNFs, or a flexible hydrated hemicellulose shell found on Holo-CNFs, would prevent this locally. The repulsive force means that the hydration layer would favorably reform if possible, probably requiring a long time due to the limited accessibility between two tightly associated surfaces.

The influence of individual hydrogen bonds on the adhesion between fibrils is indeed limited due to the lack of favorable bond energy. However, the effect of large hydrogen-bonded networks possibly formed during drying cannot be disregarded, as their numbers make it unlikely that they will all break simultaneously, simply due to probability. Another key factor will be the size of the regions where water molecules have been forced away during drying. This concept is further explored in a recent work (Wohlert et al., 2021) and put into context of the hornification process, it means that a gradual diffusion of water back is required, which takes a very long time.

Solvophobic effects might be reasonable for native uncharged cellulose and has recently been discussed in detail (Medronho, Romano, Miguel, Stigsson, & Lindman, 2012) as a plausible explanation to why cellulose is not soluble in water. However, when discussing the interactions between cellulose fibrils or fibril aggregates in the presence of water, these interactions must be treated with great care, especially for fibrils from wood, having a square crossection (Fengel & Wegener, 1984). These materials are very easily hydrated from moist air as shown by a high adsorption enthalpy of water molecules to cellulose (Hollenbeck, Peck, & Kildsig, 1978), and cellulose is also easily wetted by condensed water as demonstrated by a high cosθ, i.e. at lower contact angles, for water/cellulose interactions. (Gunnars, Wågberg, & Cohen Stuart, 2002) This means that cellulose fibrils and cellulose aggregates are highly hydrophilic, which will also result in a repulsive osmotic pressure as hydrated cellulose surfaces are brought close together in water, which in turn means that solvophobic effects most likely can be neglected for the development of the pseudo-irreversible interactions detected in the present work. Non-charged nanofibrils and fibril aggregates will indeed aggregate in aqueous dispersion but this is due to the attractive van der Waals interactions between the entities once they are brought together by Brownian motions. Thus, hornification does not seem to be an organization of the cellulose per se, rather it is likely an effect of increased molecular contact/entanglements during drying. This in turn can be reversible over a very long time in water.

3. Conclusion

The present study shows that films prepared from CNFs are suitable for studying interfibrillar interactions associated with irreversible cellulose aggregation. By relating the extent of hornification to the reswelling degree after heat treatment, a link between the extent of hornification, changes in network structure, and possible molecular interactions could be established. The main findings are that aging in ordered (semi-crystalline) and disordered cellulose systems show a pronounced heating time and temperature dependence. XPS and MVA-FTIR measurements suggest that covalent bond formation cannot be neglected when drying at 150 °C, however it was detected as highly unlikely to be the cause of hornification below this temperature. Furthermore, the lateral sizes of fibril aggregates are significantly increased when the CNF films are dried at 150 °C, although hornification occurs below this severe drying. Structural changes upon aging are reflected in wet state tensile properties but not in the dry state, which could be attributed to the contribution from reversible interactions, which are also present in the dry state. However, only in the wet state do the irreversible contacts dominate. The continuous increase of the reswelling degree on longer time scales highlights the importance of repenetration of water after the hornification process, although it remains unclear whether the process is entirely reversible. It also suggests an extremely slow accessibility to hornified regions, where the diffusion of water back in is kinetically limited. Complete reversibility can take infinite time and will remain unknown. Notably, the entangled network of fibrils (Benselfelt et al., 2023) also prevents complete dissociation so that even if hornification of these materials is entirely reversible, the material may not disperse without agitation. It has been shown that agitation of these samples is enough to separate the fibrils into a dispersed state. (Nordenström et al., 2021).

Thus, a conceptual model to explain the obtained results has emerged in which the diffusion of water plays a significant role in the hornification process. When water is expelled at elevated temperatures, close contact is formed with intermolecular interactions between cellulose molecules. For water to reenter and exchange these interactions, many weak intermolecular interactions must be exchanged simultaneously, which is unlikely but will gradually happen over a very long time. This is because there is no apparent thermodynamic gain for either state other than a minor increase in entropy upon swelling, and hence it is a slow diffusion-limited process.

4. Experimental

4.1. Chemicals

Hydrochloric acid (HCl) 37 % and sodium bicarbonate ≥99.7 % were purchased from Thermo Fischer Scientific. The chloride salt of magnesium (II), lithium (I) and cesium (I) as well as sodium carbonate ≥99.5 % were purchased from Sigma-Aldrich (Sweden). All chemicals were used as received and ultrapure water (Merck Milli-Q 18.2 MΩ/cm) or deionized water was used throughout all experiments.

4.2. Preparation of cotton linters

The cotton linters were supplied by Tumba Bruk and used as received, with a cellulose content of 99.9 % according to the calculation method of Janson. (Janson, 1974) The carbohydrate composition obtained through acid hydrolysis is provided in the Supporting information.

4.3. Preparation of carboxymethylated CNF (CM-CNF)

Carboxymethylated cellulose nanofibers were purchased from RISE Bioeconomy (Stockholm, Sweden), prepared according to the procedure of Wågberg et al. (Wågberg et al., 2008) The obtained gel was homogenized with a high-pressure Microfluidizer (Microfluidizer M-110EH, Microfluidics Corp.) through 200/100 μm chambers for three passages at approximately 1650 bar. The CNF gel was further diluted with ultrapure water to approximately 0.2%*w*/w dispersions using an IKA Ultra-Turrax high-shear mixer (12,000 rpm, 15 min). The dispersion (200 mL) was probe sonicated (amplitude 80 %, 10 min) using a VCX 750 probe sonication (diameter 13 mm) while placed in an ice bath. This was followed by centrifugation (4500 rpm, 1 h) using a Mega Star 1.6R centrifuge from VWR, and the supernatant was subsequently collected. Overnight drying of known amounts of dispersion was used to calculate

the dry content of the final dispersions (105 °C, three replicates). The average surface charge density was estimated to 534 ± 11 μmol/g and measured by polyelectrolyte titration at pH 6–7 against polydiallyldimethylammonium chloride using a ParticleMetrix Stabino (Germany) system. Three replicates were taken for each dispersion, and the average value was reported.

4.4. Preparation of CNF-Na^+ and ion-exchanged films

CNF films with different counterions were prepared following the procedure of Benselfelt et al.(Benselfelt et al., 2018; Benselfelt, Nordenström, Lindström and Wågberg, 2019) The films were formed by overnight vacuum filtration of aqueous 0.2%w/w dispersions, containing 400 mg of dry mass, on an 8 cm in diameter Durapore filter with pore size 0.65 μm, which were further dried in a Rapid-Köthen sheet dryer (Paper Testing Instruments, Austria) at a reduced pressure of 95 kPa and 93 °C for 20 min.

Upon vacuum filtration of the CNF dispersion, a thick wet gel (1–2 mm) is formed, which was soaked in aqueous 0.1 M LiCl, CsCl, $MgCl_2$ or HCl (pH 2) solutions (300 mL each) for 3 h to ion-exchange from Na^+ to the corresponding cation. The films were then washed three times in ultrapure water and subsequently dried in a Rapid-Köthen sheet dryer (Paper Testing Instruments, Austria) at a reduced pressure of 95 kPa and 93 °C for 20 min.

CNF-H^+ films that after heat treatment (130 °C, 60 min) were ion-exchanged back to Na^+ were done so by placing the dry CNF-H^+ films in a carbonate-bicarbonate buffer at pH 10.6–10.8 for 3 h, followed by washing and equilibrating in ultrapure water.

4.5. Preparation of hemicellulose-rich CNF (Holo-CNF)

Holo-CNF gel obtained through peracetic acid delignification of spruce wood chips were kindly provided by Xuan Yang et al. (Yang et al., 2019) at a concentration of approximately 0.6%w/w. The Holo-CNFs are reported to have a hemicellulose content of 26–29 % (Yang et al., 2019), the reader is referred to the original publication for the complete carbohydrate composition analysis. These were diluted with ultrapure water to 0.2%w/w dispersions and mixed using an IKA Ultra-Turrax high-shear mixer (12,000 rpm, 15 min) and subsequently, films were made containing 400 mg Holo-CNF, as described above. The surface charge density was estimated to 132 ± 33 μmol/g by polyelectrolyte titration at pH 6–7 against polydiallyldimethylammonium chloride using a ParticleMetrix Stabino (Germany) system. Three replicates were taken for each dispersion, and the average value was reported.

4.6. Swelling measurements

0.5 × 0.5 cm^2 square films were cut out. Upon heat treatment, the films were immersed in water and allowed to equilibrate for a minimum of 24 h before measurement. The films swelled uniaxially out-of-plane, and the final swelling thickness was measured with a thickness gauge.

Only the out-of-plane swellings were measured since it was found orders of magnitude larger than the in-plane-swelling.

The swelling was estimated from the change in thickness of CNF films and the swelling degree was measured as the ratio between the swelling and dry thicknesses:

$$Swelling\ degree = \frac{d_{wet} - d_{dry}}{d_{dry}}$$

Where d_{wet} and d_{dry} are the swelled and dry thickness of the films, respectively. (Benselfelt et al., 2018) The reswelling after heat treatment is the value of the swelling degree normalized against a reference sample that was not heat treated.

4.7. Mechanical analysis

Tensile tests were performed using a universal testing machine (Instron 5944). A load cell of 500 N was used for all tensile tests. Samples were 3–4 mm in width with a gauge length of 20 mm. The tests were performed at a strain rate of 2 mm min^{-1}. For each sample, 5 specimens each were tested. All dry samples were conditioned at a relative humidity (RH) of 50 % and temperature of 23 °C for 72 h before testing. Similarly, the wet CNF samples were immersed in Milli-Q water for at least 72 h before testing. The measurements were performed at 50 % RH for both dry and wet samples. The dimensions of the samples were measured with a thickness gauge and calliper before and after swelling. For the wet films, the cross-sectional area in the water-swollen state was used for evaluation.(Walther et al., 2020) The modulus was calculated as the slope of the curve in the strain interval 0–0.5 % for dry samples and 0–1 % for wet samples. (Benselfelt et al., 2018).

4.8. CP/MAS ^{13}C NMR

Cross-Polarization Magic Angle Spinning Carbon-13 Nuclear Magnetic Resonance Spectra. All samples were packed uniformly in a zirconium oxide rotor. Water swollen samples had a water content of 40 % to 60 %. The CP/MAS ^{13}C NMR spectra were recorded in a Bruker Avance III AQS 400 SB instrument operating at 9.4 T. All measurements were carried out at 295 (±1) K with a magic angle spinning (MAS) rate of 10 kHz. A 4-mm double air-bearing probe was used. Data acquisition was performed using a cross-polarization (CP) pulse sequence, i.e., a 3.15 microseconds proton 90-degree pulse, 800 microseconds ramped (100–50 %) falling contact pulse, with a 2.5 s delay between repetitions. A SPINAL64 pulse sequence was used for ^1H decoupling. The Hartmann-Hahn matching procedure was based on glycine. The chemical shift scale was calibrated to the TMS-scale (tetramethylsilane, $(CH_3)_4Si$) by assigning the data point of maximum intensity in the alpha-glycine carbonyl signal to a shift of 176.03 ppm. (Harris, 1983) 4096 transients were recorded on each sample leading to an acquisition time of about 3 h. The software for spectral fitting was developed at Innventia AB and is based on a Levenberg-Marquardt algorithm. (Larsson et al., 1997) The computations of average fibril dimension, the average fibril aggregate dimension and the average crystallinity are based on integrated signal intensities obtained from spectral fitting. (Wickholm, Larsson, & Iversen, 1998) The errors given for parameters obtained from the fitting procedure are the standard error with respect to the quality of the fit.

4.9. Wide-angle X-ray scattering

WAXS measurements were performed on an Anton Paar SAXSpoint 2.0 system (Anton Paar, Graz, Austria) equipped with a Microsource X-ray source (Cu Kα radiation, wavelength 0.15418 nm) and a Dectris 2D CMOS Eiger R 1 M detector with 75 by 75 μm pixel size. All measurements were performed with a beam size of about 500 μm in diameter, at a sample stage temperature of 25 °C with a beam path pressure at 1–2 mBar. The sample to detector distance (SDD) was 112 mm. Samples were mounted on a Solids Sampler Holder mounted on a VarioStage (Anton Paar, Graz, Austria) as dry CNF films. The dry samples were exposed to the vacuum in the beam path. 6 frames each of 30 min duration were recorded, giving a total measurement time of 180 min per sample. The transmittance was determined and used for scaling of the scattering intensities. Binning was used to generate graphs with between 500 and 510 data points, which were used for graphs and modelling. The software used for instrument control was SAXSdrive version 2.01.224 (Anton Paar, Graz, Austria), and post-acquisition data processing was performed using the software SAXSanalysis version 3.00.042 (Anton Paar, Graz, Austria).

4.10. Fourier transform infrared spectroscopy

FTIR spectra were collected on a Perkin Elmer Spectrum 100 FT-IR Spectrometer equipped with an attenuated total reflection (ATR) Golden Gate (Graseby Specac) featuring a diamond ATR crystal. All samples were analysed in the spectral region 4000–600 cm^{-1} with a spectral resolution of 4 cm^{-1} and 32 scans.

4.11. Multivariate statistical analysis

A multivariate analysis (MVA) was applied to FTIR spectral data of CNF films (only Na^+, H^+ and Holo), the analysis used follows the same procedure as Nylander et al. (Nylander et al., 2019) A principal component analysis (PCA) and orthogonal projection to latent structures (OPLS) were used in the MVA procedure. A detailed description is provided in the Supporting Information. The heating time and temperature, for the respective CNF composition samples, were used as the y-values in the MVA software against the spectral profiles. The spectral features between 2800 and 2000 cm^{-1} were excluded from the MVA. A total of 111 different samples were included in the analysis. The software SIMCA (version 16.0.2, Sartorius Stedim Data Analytics AB Umetrics, Umeå, Sweden) was used for all processing.

4.12. X-ray photoelectron spectroscopy

XPS spectra were attained with a Kratos Axis Ultra DLD electron spectrometer using monochromated Al Kα source operated at 150 W. Analyser pass energy of 160 eV for acquiring survey spectra and a pass energy of 20 eV for individual photoelectron lines were used. The surface potential was stabilized by the spectrometer charge neutralization system. The binding energy (BE) scale was referenced to the C 1 s line of aliphatic carbon, set at 285.0 eV. Processing of the spectra was accomplished with the Kratos software. To avoid possible X-ray degradation effects, C 1s and O 1s spectra were acquired first within 10 min before survey spectrum and spectra of minor elements.

Declaration of competing interest

The authors declare that they have no known competing financial interests or personal relationships that could have appeared to influence the work reported in this paper.

Data availability

Experimental data from this study are available from the corresponding authors upon request.

Acknowledgments

The Knut and Alice Wallenberg Research Foundation (KAW) are acknowledged for funding through the Wallenberg Wood Science Center. Dr. Xuan Yang is thanked for providing Holo-CNFs. The authors acknowledge the technical assistance of Dr. Andrey Shchukarev at the XPS Platform at Department of Chemistry, Umeå University. The authors are thankful for the support of Treesearch through the Research Infrastructure access program. Prof. Gunnar Westman from Chalmers University of Technology as well as Dr. Mats Josefson and Dr. Olof Svensson from Astra Zeneca are acknowledged for their contributions to the multivariate analysis.

CRediT authorship contribution statement

Farhiya Alex Sellman - Methodology, Validation, Formal analysis, Investigation, Data curation, Visualization, Writing - original draft, review and editing.

Tobias Benselfelt – Conceptualization, Methodology, Supervision, Writing – original draft, review and editing, Visualization.

Per Tomas Larsson – Methodology, Supervision, Writing – review and editing.

Lars Wågberg - Conceptualization, Methodology, Resources, Supervision, Writing- review and editing, Project administration and Funding acquisition.

Appendix A. Supplementary data

Supplementary data to this article can be found online at https://doi.org/10.1016/j.carbpol.2023.121132.

References

Ahn, K., Zaccaron, S., Zwirchmayr, N. S., Hettegger, H., Hofinger, A., Bacher, M., … Rosenau, T. (2019). Yellowing and brightness reversion of celluloses: CO or COOH, who is the culprit? *Cellulose, 26*, 429–444.

Ansari, F., Sjöstedt, A., Larsson, P. T., Berglund, L. A., & Wågberg, L. (2015). Hierarchical wood cellulose fiber/epoxy biocomposites–Materials design of fiber porosity and nanostructure. *Composites Part A: Applied Science and Manufacturing, 74*, 60–68.

Back, E., & Klinga, L. (1963a). The effect of heat treatment on internal stresses and permanent dimensional changes of paper. *Tappi, 46*(5), 284–288.

Back, E., & Klinga, L. (1963b). Reactions in dimensional stabilization of paper and fibre building board by heat treatment. *Svensk Papperstidning, 66*, 745–753.

Benselfelt, T., Engström, J., & Wågberg, L. (2018). Supramolecular double networks of cellulose nanofibrils and algal polysaccharides with excellent wet mechanical properties. *Green Chemistry, 20*(11), 2558–2570.

Benselfelt, T., Kummer, N., Nordenström, M., Fall, A. B., Nyström, G., & Wågberg, L. (2023). The colloidal properties of nanocellulose. *ChemSusChem, 16*(8), Article e202201955.

Benselfelt, T., Nordenström, M., Hamedi, M. M., & Wågberg, L. (2019). Ion-induced assemblies of highly anisotropic nanoparticles are governed by ion–ion correlation and specific ion effects. *Nanoscale, 11*(8), 3514–3520.

Benselfelt, T., Nordenström, M., Lindström, S. B., & Wågberg, L. (2019). Explaining the exceptional wet integrity of transparent cellulose nanofibril films in the presence of multivalent ions—Suitable substrates for biointerfaces. *Advanced Materials Interfaces, 6*(13), 1900333.

Benselfelt, T., & Wagberg, L. (2019). Unidirectional swelling of dynamic cellulose nanofibril networks: A platform for tunable hydrogels and aerogels with 3D shapeability. *Biomacromolecules, 20*(6), 2406–2412.

Bristow, J. A., & Kolseth, P. (1986). *Paper structure and properties: M. Dekker*.

Butchosa, N., & Zhou, Q. (2014). Water redispersible cellulose nanofibrils adsorbed with carboxymethyl cellulose. *Cellulose, 21*, 4349–4358.

Čabalová, I., Kačík, F., Geffert, A., & Kačíková, D. (2011). The effects of paper recycling and its environmental impact. *Environmental management in practice, 17*, 329–350.

Crank, J. (1979). *The mathematics of diffusion*. Oxford university press.

Fengel, D., & Wegener, G. (1984). Wood: Chemistry, ultrastructure. *Reactions, 613*, 1960–1982.

Fernandes Diniz, J., Gil, M., & Castro, J. (2004). Hornification—Its origin and interpretation in wood pulps. *Wood Science and Technology, 37*(6), 489–494.

Flory, P. J. (1942). Thermodynamics of high polymer solutions. *The Journal of Chemical Physics, 10*(1), 51–61.

Flory, P. J. (1953). *Principles of polymer chemistry*. Cornell university press.

Garg, M., Linares, M., & Zozoulenko, I. (2020). Theoretical rationalization of self-assembly of cellulose nanocrystals: Effect of surface modifications and counterions. *Biomacromolecules, 21*(8), 3069–3080.

Grignon, J., & Scallan, A. (1980). Effect of pH and neutral salts upon the swelling of cellulose gels. *Journal of Applied Polymer Science, 25*(12), 2829–2843.

Gunnars, S., Wågberg, L., & Cohen Stuart, M. (2002). Model films of cellulose: I. Method development and initial results. *Cellulose, 9*, 239–249.

Harris, R. (1983). *Nuclear magnetic resonance spectroscopy*. INC, London: Pitman Pub.

Hatton, F., Engström, J., Forsling, J., Malmström, E., & Carlmark, A. (2017). Biomimetic adsorption of zwitterionic–xyloglucan block copolymers to CNF: Towards tailored super-absorbing cellulose materials. *RSC Advances, 7*(24), 14947–14958.

Hollenbeck, R. G., Peck, G. E., & Kildsig, D. O. (1978). Application of immersional calorimetry to investigation of solid–liquid interactions: Microcrystalline cellulose–water system. *Journal of Pharmaceutical Sciences, 67*(11), 1599–1606.

Hubbe, M. A., Venditti, R. A., & Rojas, O. J. (2007). What happens to cellulosic fibers during papermaking and recycling? A review. *BioResources, 2*(4), 739–788.

Huggins, M. L. (1941). Solutions of long chain compounds. *The Journal of Chemical Physics, 9*(5), 440.

Hult, E.-L., Larsson, P., & Iversen, T. (2001). Cellulose fibril aggregation—An inherent property of kraft pulps. *Polymer, 42*(8), 3309–3314.

Idström, A., Brelid, H., Nydén, M., & Nordstierna, L. (2013). CP/MAS 13C NMR study of pulp hornification using nanocrystalline cellulose as a model system. *Carbohydrate Polymers, 92*(1), 881–884.

Israelachvili, J., & Wennerström, H. (1996). Role of hydration and water structure in biological and colloidal interactions. *Nature, 379*(6562), 219–225.

Janson, J. (1974). Analytik der polysaccharide in Holz und Zellstoff. *Faserforschung und Textiltechnik, 25*, 379–380.

Karlsson, R.-M. P., Larsson, P. T., Hansson, P., & Wågberg, L. (2019). Thermodynamics of the water-retaining properties of cellulose-based networks. *Biomacromolecules, 20*(4), 1603–1612.
Karlsson, R.-M. P., Larsson, P. T., Yu, S., Pendergraph, S. A., Pettersson, T., Hellwig, J., & Wågberg, L. (2018). Carbohydrate gel beads as model probes for quantifying non-ionic and ionic contributions behind the swelling of delignified plant fibers. *Journal of Colloid and Interface Science, 519*, 119–129.
Kato, K., & Cameron, R. (1999). A review of the relationship between thermally-accelerated ageing of paper and hornification. *Cellulose, 6*(1), 23–40.
Köhnke, T., Lund, K., Brelid, H., & Westman, G. (2010). Kraft pulp hornification: A closer look at the preventive effect gained by glucuronoxylan adsorption. *Carbohydrate Polymers, 81*(2), 226–233.
Laivins, G., & Scallan, A. (1993). The mechanism of hornification of wood pulps. In *, 2. Products of papermaking* (p. 1235).
Larsson, P. T., Wickholm, K., & Iversen, T. (1997). A CP/MAS13C NMR investigation of molecular ordering in celluloses. *Carbohydrate Research, 302*(1–2), 19–25.
Li, H., Kruteva, M., Mystek, K., Dulle, M., Ji, W., Pettersson, T., & r., & Wågberg, L.. (2020). Macro-and microstructural evolution during drying of regenerated cellulose beads. *ACS Nano, 14*(6), 6774–6784.
Liang, C., & Marchessault, R. (1959). Infrared spectra of crystalline polysaccharides. I. Hydrogen bonds in native celluloses. *Journal of Polymer Science, 37*(132), 385–395.
Lichtenstein, K., & Lavoine, N. (2017). Toward a deeper understanding of the thermal degradation mechanism of nanocellulose. *Polymer Degradation and Stability, 146*, 53–60.
Lindström, T., & Carlsson, G. (1982). The effect of chemical environment on fiber swelling. *Svensk Papperstindning-Nordisk Cellulosa, 85*(3), 14–20.
Maeda, N., Chen, N., Tirrell, M., & Israelachvili, J. N. (2002). Adhesion and friction mechanisms of polymer-on-polymer surfaces. *Science, 297*(5580), 379–382.
Medronho, B., Romano, A., Miguel, M. G., Stigsson, L., & Lindman, B. (2012). Rationalizing cellulose (in) solubility: Reviewing basic physicochemical aspects and role of hydrophobic interactions. *Cellulose, 19*, 581–587.
Missoum, K., Bras, J., & Belgacem, M. N. (2012). Water redispersible dried nanofibrillated cellulose by adding sodium chloride. *Biomacromolecules, 13*(12), 4118–4125.
Moser, C., Henriksson, G., & Lindström, M. (2018). Improved dispersibility of once-dried cellulose nanofibers in the presence of glycerol. *Nordic Pulp & Paper Research Journal, 33*(4), 647–650.
Newman, R. H. (2004). Carbon-13 NMR evidence for cocrystallization of cellulose as a mechanism for hornification of bleached kraft pulp. *Cellulose, 11*(1), 45–52.
Nordenström, M., Kaldéus, T., Erlandsson, J., Pettersson, T., Malmström, E., & Wågberg, L. (2021). Redispersion strategies for dried cellulose nanofibrils. *ACS Sustainable Chemistry & Engineering, 9*(33), 11003–11010.
Nylander, F., Svensson, O., Josefson, M., Larsson, A., & Westman, G. (2019). New features of arabinoxylan ethers revealed by using multivariate analysis. *Carbohydrate Polymers, 204*, 255–261.
Oksanen, T., Buchert, J., & Viikari, L. (1997). *The role of hemicelluloses in the hornification of bleached Kraft pulps*.
Paajanen, A., Zitting, A., Rautkari, L., Ketoja, J. A., & Penttilä, P. A. (2022). Nanoscale mechanism of moisture-induced swelling in wood microfibril bundles. *Nano Letters, 22*(13), 5143–5150.
Pantze, A. (2006). Studies of ester formation on a cellulose matrix. *Luleå tekniska universitet*, 8–16.
Peng, Y., Gardner, D. J., & Han, Y. (2012). Drying cellulose nanofibrils: In search of a suitable method. *Cellulose, 19*, 91–102.
Peng, Y., Gardner, D. J., Han, Y., Kiziltas, A., Cai, Z., & Tshabalala, M. A. (2013). Influence of drying method on the material properties of nanocellulose I: Thermostability and crystallinity. *Cellulose, 20*, 2379–2392.
Penttilä, P. A., Zitting, A., Lourençon, T., Altgen, M., Schweins, R., & Rautkari, L. (2021). Water-accessibility of interfibrillar spaces in spruce wood cell walls. *Cellulose, 28*(18), 11231–11245.
Pönni, R., Rautkari, L., Hill, C. A., & Vuorinen, T. (2014). Accessibility of hydroxyl groups in birch kraft pulps quantified by deuterium exchange in D 2 O vapor. *Cellulose, 21*(3), 1217–1226.
Quiévy, N., Jacquet, N., Sclavons, M., Deroanne, C., Paquot, M., & Devaux, J. (2010). Influence of homogenization and drying on the thermal stability of microfibrillated cellulose. *Polymer Degradation and Stability, 95*(3), 306–314.
Reid, M. S., Kedzior, S. A., Villalobos, M., & Cranston, E. D. (2017). Effect of ionic strength and surface charge density on the kinetics of cellulose nanocrystal thin film swelling. *Langmuir, 33*(30), 7403–7411.
Ritger, P. L., & Peppas, N. A. (1987). A simple equation for description of solute release I. Fickian and non-fickian release from non-swellable devices in the form of slabs, spheres, cylinders or discs. *Journal of Controlled Release, 5*(1), 23–36.
Saito, T., Hirota, M., Tamura, N., Kimura, S., Fukuzumi, H., Heux, L., & Isogai, A. (2009). Individualization of nano-sized plant cellulose fibrils by direct surface carboxylation using TEMPO catalyst under neutral conditions. *Biomacromolecules, 10*(7), 1992–1996.
Saito, T., Kimura, S., Nishiyama, Y., & Isogai, A. (2007). Cellulose nanofibers prepared by TEMPO-mediated oxidation of native cellulose. *Biomacromolecules, 8*(8), 2485–2491.
Salmén, L., & Stevanic, J. S. (2018). Effect of drying conditions on cellulose microfibril aggregation and "hornification". *Cellulose, 25*(11), 6333–6344.
Scherrer, P. (1918). Nachr Ges wiss goettingen. *Mathematical Physics, 2*, 98–100.
Sjöstedt, A., Wohlert, J., Larsson, P. T., & Wågberg, L. (2015). Structural changes during swelling of highly charged cellulose fibres. *Cellulose, 22*, 2943–2953.
Sun, R., Sun, X., & Tomkinson, J. (2004). *Hemicelluloses and their derivatives*.
Takamura, N. (1968). *Studies on hot pressing and drying process in the production of fibre board. III softening of fiber components in hot pressing of fibre mat.* 木材学会. *14(2)* p. 75).
VanderHart, D. L., & Atalla, R. (1984). Studies of microstructure in native celluloses using solid-state carbon-13 NMR. *Macromolecules, 17*(8), 1465–1472.
Wågberg, L., Decher, G., Norgren, M., Lindström, T., Ankerfors, M., & Axnäs, K. (2008). The build-up of polyelectrolyte multilayers of microfibrillated cellulose and cationic polyelectrolytes. *Langmuir, 24*(3), 784–795.
Walther, A., Lossada, F., Benselfelt, T., Kriechbaum, K., Berglund, L., Ikkala, O., … Bergström, L. (2020). Best practice for reporting wet mechanical properties of nanocellulose-based materials. *Biomacromolecules, 21*(6), 2536–2540.
Wickholm, K., Larsson, P. T., & Iversen, T. (1998). Assignment of non-crystalline forms in cellulose I by CP/MAS 13C NMR spectroscopy. *Carbohydrate Research, 312*(3), 123–129.
Wohlert, M., Benselfelt, T., Wågberg, L., Furó, I., Berglund, L. A., & Wohlert, J. (2021). Cellulose and the role of hydrogen bonds: Not in charge of everything. *Cellulose*, 1–23.
Wohlert, M., Benselfelt, T., Wågberg, L., Furó, I., Berglund, L. A., & Wohlert, J. (2022). Cellulose and the role of hydrogen bonds: Not in charge of everything. *Cellulose, 29*(1), 1–23.
Xia, J., Zhang, Z., Liu, W., Li, V. C., Cao, Y., Zhang, W., & Deng, Y. (2018). Highly transparent 100% cellulose nanofibril films with extremely high oxygen barriers in high relative humidity. *Cellulose, 25*(7), 4057–4066.
Yang, X., Berthold, F., & Berglund, L. A. (2018). Preserving cellulose structure: Delignified wood fibers for paper structures of high strength and transparency. *Biomacromolecules, 19*(7), 3020–3029.
Yang, X., Reid, M. S., Olsén, P., & Berglund, L. A. (2019). Eco-friendly cellulose nanofibrils designed by nature: Effects from preserving native state. *ACS Nano, 14*(1), 724–735.